

The large conformational changes of Hsp90 are only weakly coupled to ATP hydrolysis

Moritz Mickler¹, Martin Hessling², Christoph Ratzke¹, Johannes Buchner^{2,3} & Thorsten Hugel^{1,3}

The molecular chaperone heat-shock protein 90 (Hsp90) is one of the most abundant proteins in unstressed eukaryotic cells. Its function is dependent on an exceptionally slow ATPase reaction that involves large conformational changes. To observe these conformational changes and to understand their interplay with the ATPase function, we developed a single-molecule assay that allows examination of yeast Hsp90 dimers in real time under various nucleotide conditions. We detected conformational fluctuations between open and closed states on timescales much faster than the rate of ATP hydrolysis. The compiled distributions of dwell times allow us to assign all rate constants to a minimal kinetic model for the conformational changes of Hsp90 and to delineate the influence of ATP hydrolysis. Unexpectedly, in this model ATP lowers two energy barriers almost symmetrically, such that little directionality is introduced. Instead, stochastic, thermal fluctuations of Hsp90 are the dominating processes.

The molecular chaperone Hsp90 is responsible for the stabilization and activation of many key regulatory proteins such as the tumor-suppressor factor p53, steroid hormone receptors, kinases and various unrelated proteins identified during the past decade. Its function is dependent on ATP binding and ATP hydrolysis, although it is still unclear how ATP affects the suggested conformational changes of Hsp90 (reviewed in refs. 1–3). In addition, it has an important role in diseases, especially cancer, where the chaperoning of mutated and overexpressed oncoproteins is crucial⁴. Therefore, Hsp90 has recently become the target for a new type of anticancer drugs that specifically inhibit the ATPase function of Hsp90 (ref. 4).

The crystal structures of the Hsp90 dimer in an open and a closed conformation^{5,6} provide a good static picture and suggest that large structural changes occur during the ATPase cycle. Even though considerable progress has been made toward understanding the mechanochemical cycle of Hsp90, a clear dynamic picture is still missing^{1,3,7–9}. Especially remarkable is the slow ATPase rate for yeast Hsp90 of less than one hydrolysis event per minute at 30 °C. Many known molecular motors have an ATPase rate of about 100 per second—four orders of magnitude faster. This is especially puzzling, as certain steps in Hsp90's ATPase cycle have already been excluded as being rate limiting¹⁰. Until now, all the measurements concerning the Hsp90 kinetics have been done in bulk, where only average values are obtained. In addition, single-molecule experiments yield distributions for the various structural states and do not require any synchronization of the system. This is especially relevant for the Hsp90 system, where the presence of several conformational states impedes the population of an unambiguously defined state in bulk. Therefore, insights into the function of Hsp90 that have been inaccessible to date are expected to be obtained using single-molecule techniques.

Here we performed single-molecule experiments to observe the conformational changes in single *Saccharomyces cerevisiae* Hsp90 dimers in real time in an aqueous environment. A thorough kinetic analysis allows us to assign all eight rate constants of a minimal kinetic model that explains the influence of ATP and other nucleotides on the conformational changes. Finally, this kinetic model is confirmed with the $\Delta 8$ mutant, which is known to double the ATPase rate and to shift the equilibrium conformation to the closed state¹¹.

RESULTS

Immobilization of single Hsp90s and smFRET detection

To address the kinetics of the mechanical cycle of yeast Hsp90, we developed a single-molecule assay that allows us to follow the conformational change of single Hsp90 dimers in real time. We engineered single-cysteine mutants of Hsp90 via site-directed mutagenesis that retain activity *in vivo*. The single cysteine on one mutant (D61C) was labeled with a donor fluorophore, Atto550, and that on the second mutant (E385C) was labeled with an acceptor fluorophore, Atto647N. After mixing the homodimers, we could observe the formation of heterodimers by the increasing acceptor fluorescence (Supplementary Fig. 1 online). These constructs were either biotinylated with N-hydroxysuccinimidobiotin (NHS-biotin) or incubated with biotinylated antibodies against a streptavidin tag that was added to the C terminus of Hsp90. To prevent dissociation of the dimer, we carried out most experiments using a Hsp90 construct with an additional coiled coil motif at the C terminus before the streptavidin tag^{12,13}. The ATPase rates of all constructs were determined by an ATP-recovering ATPase assay^{14,15} and were found to be the same as that of the wild-type Hsp90 within the error of the measurement. In

¹Physik-Department, IMETUM, CeNS, James-Frank-Strasse 1, ²Department Chemie, Lichtenbergstrasse 4, and ³Center for Integrated Protein Science CIPSM, Technische Universität München, 85748 Garching, Germany. Correspondence should be addressed to T.H. (thorsten.hugel@ph.tum.de).

Received 23 May 2008; accepted 12 January 2009; published online 22 February 2009; doi:10.1038/nsmb.1557

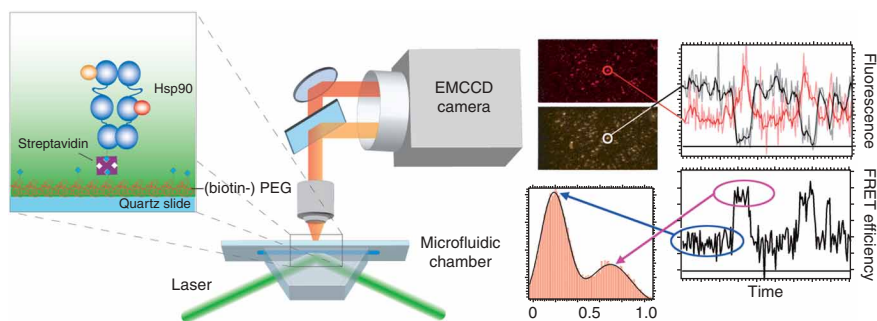


Figure 1 Experimental setup. The Hsp90 molecules were attached to a biotin-PEG surface in a microfluidic chamber, which was mounted in a prism-type TIRF microscope. Single-molecule fluorescence from the donor and acceptor were detected simultaneously by an EMCCD camera. Matching time traces were overlaid (above right) and FRET efficiencies determined (below right). Finally, the cumulated histogram of all FRET efficiencies shows two clearly separated states (arrows). See Methods.

addition, we confirmed the functionality of the constructs by measuring p23 binding (**Supplementary Fig. 2** online).

For the single-molecule measurements, the constructs were tethered to a polymer-coated quartz substrate^{16,17}. This quartz substrate is part of a microfluidic chamber that is mounted in a custom-built prism-type total internal reflection fluorescence (TIRF) microscope. We detected conformational changes by single-molecule fluorescence resonance energy transfer (smFRET)¹⁶ in solution at 30 °C. The setup allowed excitation and detection of both fluorophores in parallel or separately (see **Fig. 1** and Methods for more details).

The typical lifetime of the Atto647N fluorophore attached to Hsp90 is about 30 s in our system. Therefore, we excited the fluorophores for only 100 ms every second, if not otherwise stated. This allowed for observation times of several minutes. **Figure 2a** (above) shows an example of such a single-molecule trace with saturating ATP (black, donor; red, acceptor). The black signal (middle) represents the corrected FRET efficiency (see Methods) and the blue signal (below) represents the total intensity. A state is defined as closed if the FRET efficiency is higher than 0.5 and open if it is lower (see Methods). Thus, the traces show opening and closing of the Hsp90 dimer on timescales much faster than the time for one ATPase cycle, which is around 100 s for the construct shown here at 30 °C. To demonstrate that the changes in FRET efficiency are real conformational changes of the dimer and not photo-physical effects of the fluorophores, we took data with the highest frame rate at continuous illumination and detection (**Fig. 2b**). Again, a clear signal on the timescale of seconds can be seen. The possibility of blinking of the donor was excluded by the stability of the total fluorescence intensity (**Fig. 2a,b**, below), whereas the blinking of the acceptor as a source for this fast dynamics was excluded by alternating laser excitation (**Supplementary Fig. 3** online). Therefore, these events represent true opening and closing of Hsp90.

To exclude surface effects on the dynamics of Hsp90, we performed some of the experiments with Hsp90 caged in vesicles with a radius of about 100 nm¹⁸. These experiments result in the same FRET dynamics. A schematic of this experiment, some example traces and the dwell-time distribution are shown in **Supplementary Figure 4** online.

Influence of nucleotides and mutations

The length of time that each Hsp90 dimer stays in the open and closed state, respectively, (dwell times) provides us with information on the rate constants for the kinetic cycle (details in the next section). Integrated dwell-time distributions in the open and closed states with ATP (black), without ATP (blue) and with ATP- γ S (an ATP analog that is slowly hydrolyzed) are

given in **Figure 3**. We fit integrated rather than plain distributions, because they are independent of binning and therefore allow better data analysis¹⁹. Each distribution consists of more than 100 traces and more than 200 dwell times. On the basis of these distributions, we compiled a minimal kinetic model that reproduces the slow bulk ATPase rate for ATP and ATP- γ S as explained in the next section. ATP- γ S reduced the rate constant of ATP hydrolysis by about a factor of eight in bulk experiments of Hsp90 (data not shown).

Next we measured the distributions in the presence of exclusively 2 mM ADP or exclusively AMP-PNP (a nonhydrolyzable ATP analog, known to stabilize the N-terminal dimerization). Within the uncertainties of our measurements, the distributions without nucleotide and with ADP were the same. On the other hand, AMP-PNP changed the observed traces drastically (**Fig. 4a**). The traces consist of long closed states with no conformational fluctuations on the timescale of

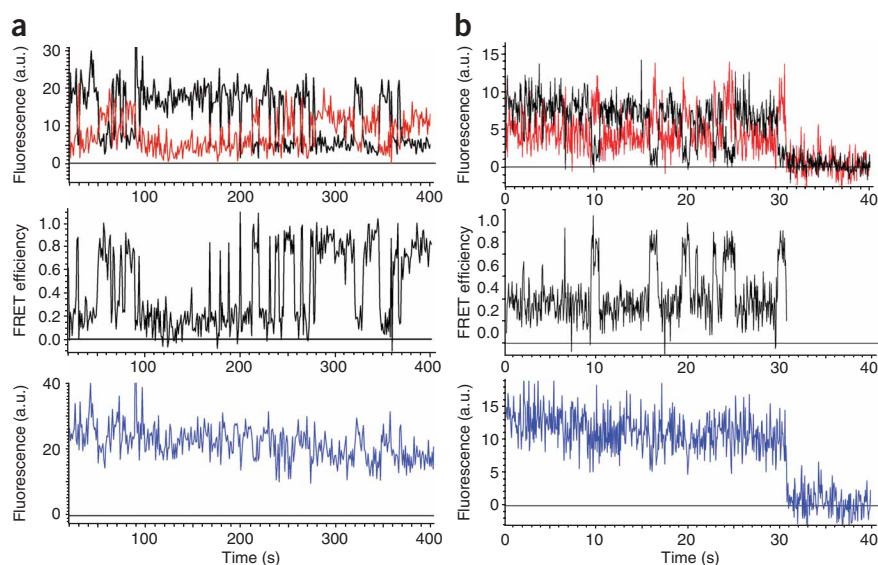


Figure 2 Single-molecule FRET time traces with ATP. Exemplary fluorescence time trace of a Hsp90 heterodimer with one frame per second (**a**) and with one frame per 55 ms (**b**). Above, fluorescence signal of the donor (black trace) and the acceptor (red trace). Bold lines correspond to a five-frame sliding average. Middle, calculated FRET efficiency. Below, total fluorescence intensity. a.u., arbitrary units.

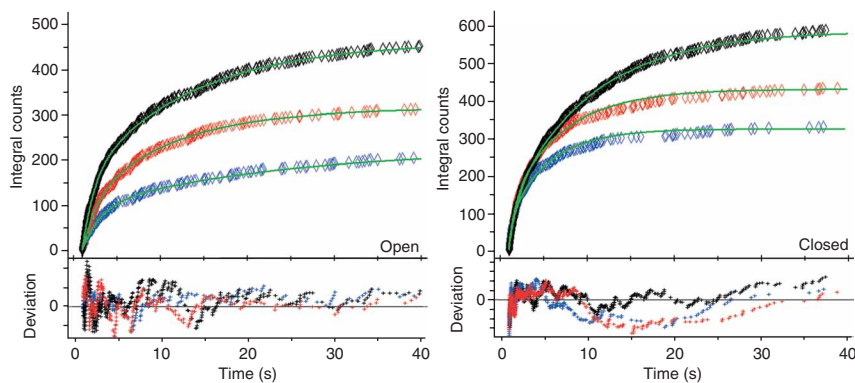


Figure 3 Dwell-time distributions for various nucleotide conditions. Integrated dwell-time distribution in the open (left) and closed (right) states. Curves with ATP (black), ATP- γ S (red) and without nucleotide or ADP (blue) are reproduced by a four-state kinetic Monte Carlo calculation (green). Deviations of the kinetic Monte Carlo calculations from the experimental data are shown below. For the calculation of the uncertainties in the rate constants, see the main text and **Figure 6a**.

seconds or tens of seconds. This suggests that Hsp90 is fixed in one of its closed conformations for many minutes, as expected from bulk experiments. We observed high FRET states up to a dwell time of 10 min, in general limited by only the bleaching of the acceptor fluorophore.

Finally, we measured the $\Delta 8$ mutant. In the absence of nucleotide, we observed dynamics on the timescale of seconds (**Fig. 4b**), similar to the dynamics of full-length Hsp90. The only substantial difference was that the dwell times in the open state were shorter (for a comparison of the dwell times of the $\Delta 8$ mutant with those of full-length Hsp90, see **Supplementary Fig. 5** online and **Supplementary Table 1** online). Addition of ATP shifted the equilibrium completely (on the timescale of our experiments) to the closed state, similarly to what was observed with AMP-PNP, resulting in traces such as those in **Figure 4c**. We could no longer detect the open state, indicating that the dwell time in the open state was less than 0.2 s (limited by the time resolution of our experimental setup) or that the closed state was trapped (see Discussion).

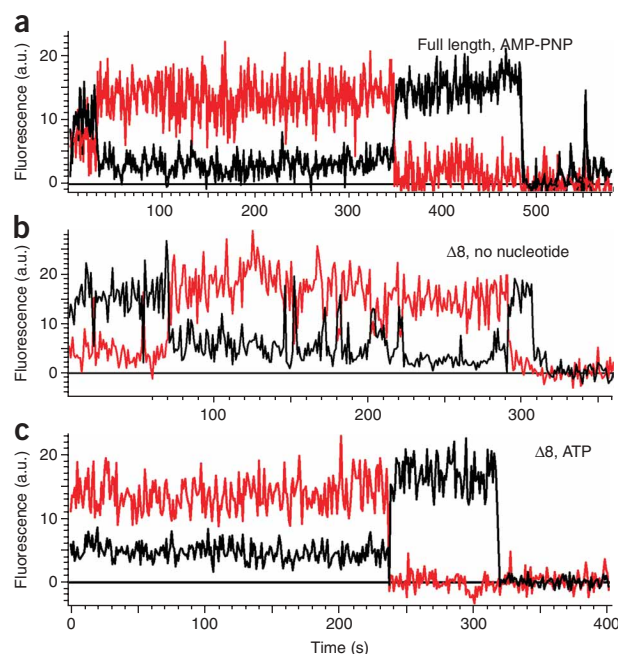
Kinetic cycle determined by Monte Carlo calculations

The integrated distributions of the open and closed times of Hsp90 (**Fig. 3**) cannot be fitted with a single exponential, but a double exponential fits the data well (χ^2 is better by more than a factor of five). Notably, a power-law fit with three parameters seems to describe the data equally well, an observation that will be addressed elsewhere. The decay times ($1/k$) were on the order of seconds and a few tens of seconds. This was unexpected, as the ATPase rate was a magnitude slower even than the slowest measured decay time. To elucidate this apparent discrepancy, we set up a minimal kinetic model for the conformational changes, in which all rate constants were determined directly from the data.

Figure 4 smFRET trace with AMP-PNP and the $\Delta 8$ mutant. (a) Typical smFRET trace of Hsp90 with the nonhydrolyzable AMP-PNP. At $t = 0$ or before, an open (low FRET) Hsp90 dimer attaches to the substrate and then closes (high FRET) at $t = 30$ s. Finally, the acceptor bleaches at $t = 350$ s (zero FRET). In almost all traces with AMP-PNP, the dimer stayed in its closed state once it was reached for the timescale of the experiment—that is, during the lifetime of the acceptor molecule. (b,c) Typical smFRET traces for the $\Delta 8$ mutant of Hsp90 without nucleotide (b) and with 2 mM ATP (c). a.u., arbitrary units.

Because a double-exponential decay can take place only if there are two distinct species, the double-exponential fit obtained here for the open as well as for the closed time distributions requires that there are two open and two closed conformations. Therefore, we can separate four different states. Guided by several biochemical and structural studies^{2,10,20}, we aligned the four states in a reaction cycle as depicted in **Figure 5** with states A and D being open (low FRET) and state B and C being closed (high FRET), resulting in eight rate constants. Several publications depict cycles with two different closed and/or two different open structures, but only one for each has been confirmed by crystal structures. Therefore, we do not speculate on any other structures here and depict the same structure for the two open (A, D) and the two closed (B, C) states, respectively.

The analytical solution of this four-state system (E. Frey, personal communication) relates the four decay times of the two double-exponential fits to the eight rate constants of the cycle. A parallel fit of these expressions to the dwell-time distributions would then give the eight rate constants. The same results can be obtained more easily from kinetic Monte Carlo calculations, which we performed as described below. The results were finally checked against the analytical expressions. We simulated the system depicted in **Figure 5** and obtained the eight rate constants by simultaneously adjusting the outcome of the kinetic Monte Carlo calculations to the two dwell-time distributions. Such a kinetic Monte Carlo calculation (a description of how such calculations are done is given in the Methods) does indeed exactly represent the system depicted in **Figure 5** with the inserted rate constants. There is no further parameter involved, and the integrated dwell-time distribution for the input system will exactly look like the outcome of the calculation (note that this is not a fit to the distribution). Uncertainties in the rate constants are extremely small



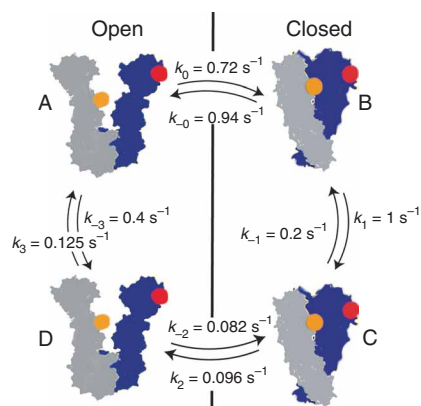


Figure 5 Minimal kinetic model. Minimal kinetic model of the conformational changes in Hsp90. States A and D are open and states B and C are closed. A sketch on the basis of the two available crystal structures illustrates possible conformations. The fluorophores are represented by the red (ATTO647N) and orange (ATTO550) spheres. The two open conformations (and likewise the two closed conformations) are indistinguishable in their FRET values, but the rate constants in between all states can be assigned from the integrated dwell-time distributions. Rate constants are given for saturating ATP concentration; for other values see **Figure 6a**.

for the large rate constants, because they dominate the system. (This follows from linear algebra: large eigenvalues of a system of differential equations dominate this system.) In turn, smaller rate constants have a larger variation, because they influence the system to a lesser degree and are more difficult to observe due to the limited lifetime of the fluorophores. We determined the uncertainties of all rate constants by changing the rate constant under investigation and adjusting all other rate constants to compensate for this change. The uncertainty is then given by the maximum change that can be compensated to have the resulting exact integrated dwell-time distribution still within the error of the measurement (an example is given in the **Supplementary Fig. 5**). Finally, **Figure 6a** gives all the rate constants and their uncertainties; please note the logarithmic scale for the rate constants. The time to proceed once through the cycle in **Figure 5** can be directly extracted from the kinetic Monte Carlo calculations. It is about 100 s for ATP and 700 s for ATP- γ S.

Kinetic Monte Carlo calculations for any three-state models could not reproduce our measured distributions. Models with more than four states (the states could be on or off pathway), can of course represent our data as well as our four-state model, but we consider such a model unlikely for Hsp90 without substrate or cochaperone, as the four-state model already represents the measured data well without any additional assumptions.

DISCUSSION

Figure 6b shows the schematics of an energy landscape representing the above calculated eight rate constants for the three different nucleotide conditions depicted in **Figure 6a** to emphasize a different viewpoint, which follows from the above data. The absolute values for the free energy are calculated from the Arrhenius equation as described in Methods, whereas the distances to the transition states are arbitrary. This representation shows clearly that all four states can be accessed without nucleotide, which is consistent with previous findings^{1,20,21}. In addition, ATP- γ S and ATP lower the two energy barriers between states B and C and between states D and A (compared to the nucleotide-free or the ADP state). The changes in these energy barriers are what mainly affect the ATPase rates, which are consistent with bulk ATPase rates (see below). Therefore, the stochastic transitions between the different states dominate the time taken to proceed through the ATPase cycle. Together, these results show that

ATP hydrolysis and the conformational cycle are not tightly coupled. In other words, there is no irreversible conformational change that requires ATP hydrolysis (although ATP hydrolysis accelerates some conformational changes and is itself, of course, irreversible).

On first sight, the lowering of two barriers might be unexpected, but one of them (probably between B and C) could result from ATP hydrolysis, whereas the release of ADP or phosphate could account for the lowering of the other barrier between the open states (A and D). Any other conformational change induced by ATP binding or hydrolysis (even in another domain) could also account for any of the barrier reductions. The weak coupling of the conformational changes to the hydrolysis makes identification of the hydrolysis step with this kind of experiment impossible. Three-color FRET experiments with labeled ATP should shed light on this issue in the future.

How does the bulk ATPase rate compare to our model? Indeed, the ATPase rate of about one per 100 s (for all our full-length constructs) is consistent with the average time to proceed once through all four states in the cycle (**Fig. 5**)—although all rate constants for the conformational change in our proposed cycle are at least an order of magnitude faster! In the case of the slowly hydrolyzing analog ATP- γ S, the bulk hydrolysis rate is reduced by a factor of eight, which is also consistent with our measured time to proceed through the cycle of about 700 s. Therefore, our kinetic cycle reproduces the bulk ATPase rate for two different nucleotide conditions under the assumption that one ATP is hydrolyzed per cycle.

How well does this kinetic model further explain previously published data? From the crystal structure⁵ and other biochemical data on Hsp90 (ref. 10), at least three²² but usually four conformational states have been suggested^{2,23,24}. A four-state model is also consistent with transmission EM images of *Escherichia coli* Hsp90 (ref. 6) and with atomic force microscopic images of MutL²⁵, which belongs to the same family as Hsp90.

The high dynamics and the accessibility of various conformations are also consistent with recent findings based on SAXS measurements

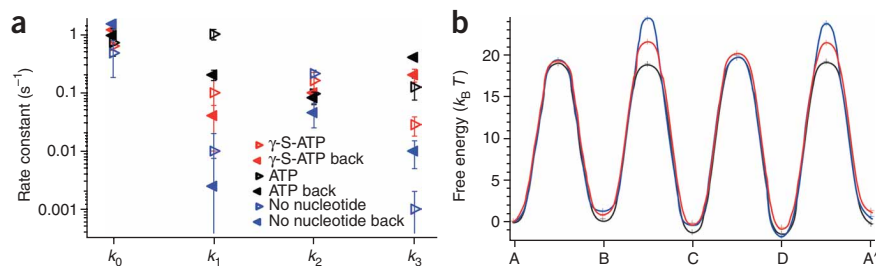


Figure 6 Rate constants, uncertainties and energy landscape. (a) Overview of the determined rate constants and their uncertainties. All determined rate constants are given in **Supplementary Table 1**. (b) Schematic energy landscape of the Hsp90 ATPase conformational states with ATP (black), with ATP- γ S (red) and without nucleotide (blue). In the presence of ATP, the energy barriers between the closed states B and C and between the open states D and A are lowered substantially compared to the situation without nucleotide. The barriers for ATP- γ S are in between.

in solution on *E. coli* Hsp90 (ref. 21). One difference compared to recent findings on the *E. coli* Hsp90 (ref. 6) is that we did not observe a distinct conformation of an ADP bound state. If this state does also exist in yeast Hsp90, it must be short lived and little populated.

Furthermore, both the single-molecule measurements with AMP-PNP (full-length construct) and with the $\Delta 8$ mutant are consistent with published results from bulk experiments. When AMP-PNP is incubated with Hsp90 and put on a sizing column, all molecules elute at the size of a dimer²⁴, the interpretation being that AMP-PNP traps the N-terminal dimerized closed state. The single-molecule traces with AMP-PNP (Fig. 4a) are consistent with this observation and interpretation. In almost all traces, we observed only the closed (high FRET) state, such as in Figure 4a where the dimer is closed for longer than our observation time, which is limited by the lifetime of our acceptor (here around 350 s). This prevented us from doing the full dwell-time analysis and extracting all the rate constants for AMP-PNP. The $\Delta 8$ mutant showed a similar behavior to the full-length Hsp90 in the absence of nucleotide, both in bulk²⁴ and in the single-molecule experiments (Fig. 4b). The dwell-time analysis shows an acceleration of about a factor of two for the rate constants k_0 and k_{-2} (that is, the transitions from the open to the closed states). This difference between the $\Delta 8$ mutant and the full-length construct becomes pronounced when ATP is added. Both the bulk elution data from sizing columns²⁴ and the single-molecule traces (Fig. 4c) of the $\Delta 8$ mutant with ATP look similar to the AMP-PNP data of the full-length construct. This consistently shows that the addition of ATP shifts the equilibrium toward the closed state, such that the open state cannot be observed anymore. The interpretation of the bulk data are an acceleration of the N-terminal dimerization, such that the open state is only short-lived²⁴. Under this assumption, we can set a lower limit on the accelerated rate constants for the $\Delta 8$ mutant in the presence of ATP. This limit is imposed by the speed of our camera, around 10 frames per second, which means that k_0 and k_{-2} must be faster than 5 per second. Or in other words, the open state is populated for less than 0.2 s during one cycle. Such a timescale is actually still not considered fast for most known molecular motors, which complete their ATPase cycles often in less than 0.1 s²⁶.

A second effect of the $\Delta 8$ mutant comes from bulk ATPase assays where we observed a doubling of the ATPase rate²⁴. In the following we speculate on how this could fit into our proposed cycle. The full-length construct spends about half the time of the ATPase cycle in the open and half in the closed state. As already pointed out, the $\Delta 8$ mutant shortens the time spent in the open state to less than 0.2 s, which makes the time spent in the open state negligible. This would result in only half the time to proceed through the cycle and could explain the molecular origin of the doubling of the ATPase rate.

Finally, our FRET data allow us to estimate the distances between the fluorophores in the open and closed state with an assumptions on their orientation ($\kappa^2 = 2/3$). This assumption is reasonable for our system with anisotropies of less than 0.2 (ref. 27). The calculated distances of the FRET pair are 8.3 nm for the open and 5.2 nm for the closed state. Considering the uncertainties in fluorophore orientation, linker flexibility and quenching, this is sufficiently close to the data from the crystal structure. We measured the distance between the C α to C α atoms in the structures PDB 2CGE and PDB 2CG9 (ref. 5) with Pymol 0.99rc6 (DeLano Scientific) and obtained values of about 7.0 nm in the open and 4.2 nm in the closed state.

In summary, our single-molecule experiments allowed us to directly observe the large conformational changes within Hsp90 that were suggested from biochemical analysis, static crystal structures and solution small-angle X-ray scattering (SAXS) measurements^{3,5,9,21,28}.

On the basis of single-molecule experiments in combination with biochemical assays and kinetic Monte Carlo calculations, we propose a minimal kinetic model in which all rate constants are assigned without any further assumptions. The model is consistent with all available bulk data but proposes a new mechanism whereby the large conformational changes of Hsp90 and its ATP hydrolysis are only weakly coupled in the absence of substrate and cochaperones. In other words, the conformational changes are dominated by stochastic (thermal) fluctuations. Our single-molecule FRET experiments on yeast Hsp90 provide insight into key dynamic mechanistic questions that could not be solved with bulk experiments. This is due to the intrinsic averaging in bulk experiments, especially in a system involving several conformational states that hamper the decomposition of the various forward and backward rate constants. Finally, the path to investigate the interplay of the observed conformational changes in Hsp90 with the binding of substrate proteins and cochaperones in real time has been opened.

METHODS

Protein expression and purification. To prevent the Hsp90 dimer from dissociation in the single-molecule experiments, we inserted a coiled coil motif of the kinesin neck region of *Drosophila melanogaster* (DmKHC) to the C terminus of Hsp90. In addition, we introduced a streptavidin tag (IBA GmbH) onto the C-terminal end for specific binding to the surface. Data for the stability of the dimerization are shown in Supplementary Figure 1.

To emphasize that these findings are not an artifact of the added coiled coil part, we performed some of the experiments without the coiled coil region. For surface-attached Hsp90 in several hundred experiments, we never observed more than one ATPase cycle (the original reason why we introduced the coiled coil), but we did observe the fast fluctuations on the timescale of seconds. Considering that bulk exchange experiments show an average monomer exchange rate that matches the bulk ATPase rate of less than one per minute, this excludes the dissociation as explanation for the fast dynamics on the timescale of few seconds. In addition, a previous study²⁹ demonstrated the function of a Hsp90 construct with a coiled coil motif in an *in vivo* system.

Cysteine point mutations and the $\Delta 8$ mutant were created with the QuickChange Multi Site-Directed Mutagenesis Kit (Stratagene). We designed the primers using the program provided on the Stratagene website. We carried out protein expression and purification as described⁹.

Labeling efficiency and scavengers. We labeled the Hsp90 cysteine mutants with the fluorescence molecules (AttoTec, Siegen) by maleimide chemistry, and determined the labeling efficiency by absorption spectra in a Nanodrop ND-1000 UV-Vis spectrometer. Finally, a labeling ratio of one fluorophore per Hsp90 monomer was achieved ($\pm 5\%$). The two common scavengers for Atto647N, namely Trolox and ROXS³⁰ did not improve the lifetime of the fluorophores in our system.

Energy landscape. We estimated the transition-barrier height of the potential-energy landscape (Fig. 6b) by means of the Arrhenius equation:

$$\Delta G^* = k_B T \ln(A/k)$$

where k is the transition rate constant from one state to the next, k_B is the Boltzmann constant, T is the temperature and A is the Arrhenius prefactor. For proteins, this factor is commonly set to $A = 10^8 \text{ s}^{-1}$ (refs. 31,32). We assumed that A does not vary significantly for the various states.

Experimental setup. We carried out all single-molecule fluorescence measurements in a custom-built prism-type TIRF microscope. The two colors for donor and acceptor fluorescence were separated and simultaneously recorded on an Andor DV887 (Andor Technology) camera at a temperature of -100°C (each color on one half of the chip; Fig. 1). We analyzed the movies with a program from the Hugel laboratory based on Igor Pro 6.01 (WaveMetrics). First, the time traces of single fluorophores were extracted from the movie with a simple threshold criterion. Then, the two colors were overlaid and the

corrected FRET efficiency was calculated²⁷ (traces above right in Fig. 1). These FRET efficiencies (every single data point) were then cumulated into a histogram (Fig. 1). As fluorescence is a stochastic process, the FRET efficiency of a single state is expected to have a Gaussian distribution. Our efficiencies can be fit nicely with two Gaussian distributions and can therefore be divided into two states separated at a transfer efficiency of 0.5. Every crossing of this threshold corresponds to a transition between the open and closed states. The overlap of the two distributions results in a mis-assignment of less than 1%.

Kinetic Monte Carlo calculations. We carried out the kinetic Monte Carlo calculations using software from the Hugel laboratory based on Igor Pro 6.01. In short, the single Hsp90 dimer was set to a defined state (for example, A) and the dimer was then allowed to access the different states with the given rate constants. The starting state is not relevant, as the conformational changes are a Markov process, and therefore memory is lost after few time steps (this was also confirmed). We did many Monte Carlo runs, varying the time steps from 0.05 s to 0.001 s and the number of steps from 100,000 to 50,000,000. All gave the same result, demonstrating that the time steps were sufficiently small and the number of steps sufficiently large. We then used the time that was spent in either state A and D (open) or state B and C (closed) to calculate the integrated dwell-time distributions, which then were directly compared to the measured data. Uncertainties were determined as described in the main text (Supplementary Fig. 6 and Supplementary Methods online). Finally, the results were checked against the analytical solution for our four-state cycle. The random numbers simulating the statistic nature of the transitions were generated by the function *enoise*.

Note: Supplementary information is available on the Nature Structural & Molecular Biology website.

ACKNOWLEDGMENTS

We thank E. Frey, R. Metzler, K. Richter and M. Rief for helpful discussions and critical reading of the manuscript and Nano Initiative Munich for financial support.

AUTHOR CONTRIBUTIONS

M.M. performed experiments and kinetic Monte Carlo calculations; M.H., M.M. and C.R. designed constructs and purified the proteins. M.M. and C.R. labeled and characterized the proteins; J.B. and T.H. planned and supervised the study; T.H. and M.M. wrote the manuscript; all authors discussed the results and commented on the manuscript.

Published online at <http://www.nature.com/nsmb/>

Reprints and permissions information is available online at <http://npg.nature.com/reprintsandpermissions/>

- Pearl, L.H. & Prodromou, C. Structure and mechanism of the Hsp90 molecular chaperone machinery. *Annu. Rev. Biochem.* **75**, 271–294 (2006).
- Richter, K. & Buchner, J. hsp90: twist and fold. *Cell* **127**, 251–253 (2006).
- Richter, K., Reinstein, J. & Buchner, J. A Grp on the Hsp90 mechanism. *Mol. Cell* **28**, 177–179 (2007).
- Whitesell, L. & Lindquist, S.L. HSP90 and the chaperoning of cancer. *Nat. Rev. Cancer* **5**, 761–772 (2005).
- Ali, M.M.U. *et al.* Crystal structure of an Hsp90-nucleotide-p23/Sba1 closed chaperone complex. *Nature* **440**, 1013–1017 (2006).
- Shiau, A.K., Harris, S.F., Southworth, D.R. & Agard, D.A. Structural analysis of *E. coli* Hsp90 reveals dramatic nucleotide-dependent conformational rearrangements. *Cell* **127**, 329–340 (2006).
- Brown, M.A., Zhu, L., Schmidt, C. & Tucker, P.W. Hsp90—from signal transduction to cell transformation. *Biochem. Biophys. Res. Commun.* **363**, 241–246 (2007).
- Siligardi, G. *et al.* Co-chaperone regulation of conformational switching in the Hsp90 ATPase cycle. *J. Biol. Chem.* **279**, 51989–51998 (2004).
- Richter, K., Muschler, P., Hainzl, O. & Buchner, J. Coordinated ATP hydrolysis by the Hsp90 dimer. *J. Biol. Chem.* **276**, 33689–33696 (2001).
- Weigl, T. *et al.* C-terminal regions of Hsp90 are important for trapping the nucleotide during the ATPase cycle. *J. Mol. Biol.* **303**, 583–592 (2000).
- Richter, K., Reinstein, J. & Buchner, J. N-terminal residues regulate the catalytic efficiency of the Hsp90 ATPase cycle. *J. Biol. Chem.* **277**, 44905–44910 (2002).
- Dietz, H., Bornschlogl, T., Heym, R., Konig, F. & Rief, M. Programming protein self assembly with coiled coils. *New J. Phys.* **9**, 424, 1–8 (2007).
- Bornschlogl, T. & Rief, M. Single-molecule dynamics of mechanical coiled-coil unzipping. *Langmuir* **24**, 1338–1342 (2008).
- Ali, J.A., Jackson, P.A., Howells, A.J. & Maxwell, A. The 43-kilodalton N-terminal fragment of the DNA gyrase B protein hydrolyzes ATP and binds coumarin drugs. *Biochemistry* **32**, 2717–2724 (1993).
- Panaretou, B. *et al.* ATP binding and hydrolysis are essential to the function of the Hsp90 molecular chaperone *in vivo*. *EMBO J.* **17**, 4829–4836 (1998).
- Ha, T. *et al.* Probing the interaction between two single molecules: fluorescence resonance energy transfer between a single donor and a single acceptor. *Proc. Natl. Acad. Sci. USA* **93**, 6264–6268 (1996).
- Hugel, T. *et al.* Experimental test of connector rotation during DNA packaging into bacteriophage phi 29 capsids. *PLoS Biol.* **5**, e59 (2007).
- Cisse, I., Okumus, B., Joo, C. & Ha, T. Fueling protein–DNA interactions inside porous nanocontainers. *Proc. Natl. Acad. Sci. USA* **104**, 12646–12650 (2007).
- Gebhardt, J.C.M., Clemen, A.E.M., Jaud, J. & Rief, M. Myosin-V is a mechanical ratchet. *Proc. Natl. Acad. Sci. USA* **103**, 8680–8685 (2006).
- Bron, P. *et al.* Apo-Hsp90 coexists in two open conformational states in solution. *Biol. Cell* **100**, 413–425 (2008).
- Krukenberg, K.A., Förster, F., Rice, L.M., Sali, A. & Agard, D.A. Multiple Conformations of *E. coli* Hsp90 in solution: insights into the conformational dynamics of Hsp90. *Structure* **16**, 755–765 (2008).
- Bracher, A. & Hartl, F.U. Hsp90 structure: when two ends meet. *Nat. Struct. Mol. Biol.* **13**, 478–480 (2006).
- Pearl, L.H., Prodromou, C. & Workman, P. The Hsp90 molecular chaperone: an open and shut case for treatment. *Biochem. J.* **410**, 439–453 (2008).
- Richter, K., Reinstein, J. & Buchner, J. N-terminal residues regulate the catalytic efficiency of the Hsp90 ATPase cycle. *J. Biol. Chem.* **277**, 44905–44910 (2002).
- Sacho, E.J., Kadyrov, F.A., Modrich, P., Kunkel, T.A. & Erie, D.A. Direct visualization of asymmetric adenine nucleotide-induced conformational changes in MutL. *Mol. Cell* **29**, 112–121 (2008).
- Howard, J. *Mechanics of Motor Proteins and the Cytoskeleton* (Sinauer, Sunderland, MA, 2001).
- Roy, R., Hohng, S. & Ha, T. A practical guide to single-molecule FRET. *Nat. Methods* **5**, 507–516 (2008).
- Jackson, S.E. The solution to multiple structures. *Structure* **16**, 659–661 (2008).
- Wayne, N. & Bolon, D.N. Dimerization of Hsp90 is required for *in vivo* function: design and analysis of monomers and dimers. *J. Biol. Chem.* **282**, 35386–35395 (2007).
- Vogelsang, J.R.K. *et al.* A reducing and oxidizing system minimizes photobleaching and blinking of fluorescent dyes. *Angew. Chem. Int. Ed. Engl.* **47**, 5465–5469 (2008).
- Lapidus, L.J., Eaton, W.A. & Hofrichter, J. Measuring the rate of intramolecular contact formation in polypeptides. *Proc. Natl. Acad. Sci. USA* **97**, 7220–7225 (2000).
- Yang, W.Y. & Gruebele, M. Folding at the speed limit. *Nature* **423**, 193–197 (2003).

Copyright of Nature Structural & Molecular Biology is the property of Nature Publishing Group and its content may not be copied or emailed to multiple sites or posted to a listserv without the copyright holder's express written permission. However, users may print, download, or email articles for individual use.